Chem

CellPress

Article

Electrostatic Stabilization of Single-Atom Catalysts by Ionic Liquids

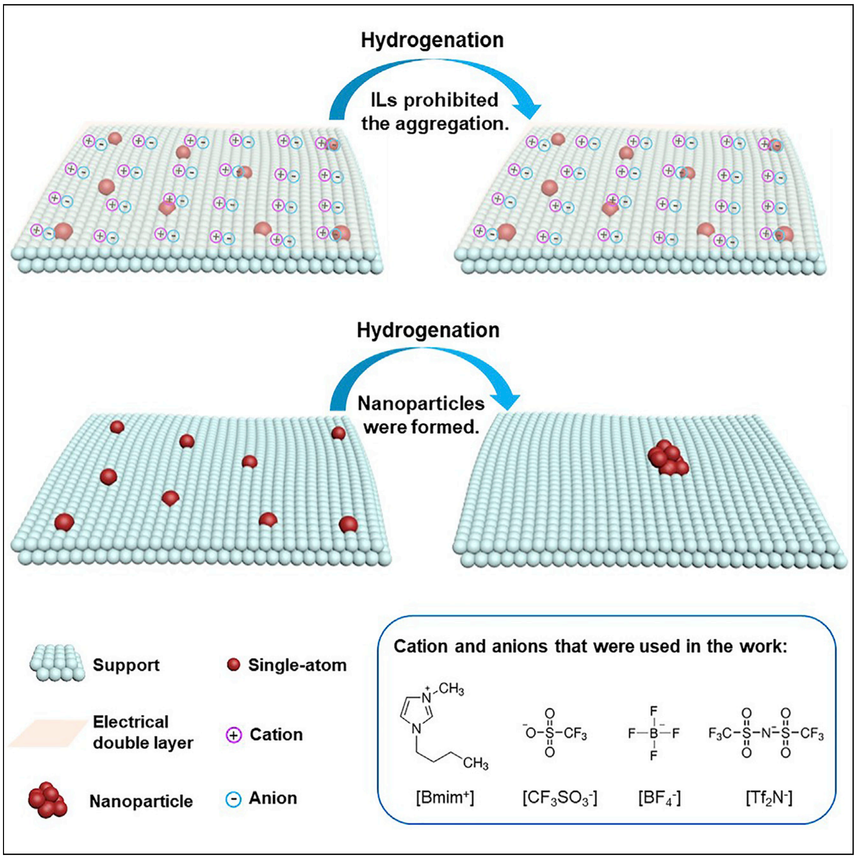

Shipeng Ding, Yalin Guo, Max J. Hülsey, ..., Botao Qiao, Tao Zhang, Ning Yan

asakura@moleng.kyoto-u.ac.jp (H.A.)
gaomin@cat.hokudai.ac.jp (M.G.)
bqiao@dicp.ac.cn (B.Q.)
ning.yan@nus.edu.sg (N.Y.)

HIGHLIGHTS

Ionic liquids sharply enhance the stability of single-atom catalysts

The nature of the increased stability is due to electrostatic interaction

The strategy is readily extendable to a variety of metal-support combinations

Electrostatic interaction has been demonstrated as a simple and general strategy to protect atomically dispersed metal catalysts. Ionic liquid-stabilized single-atom catalysts (ILSSACs) exhibited considerably enhanced durability and hydrogenation activity for a series of catalysts.

9 INDUSTRY, INNOVATION AND INFRASTRUCTURE

Ding et al., Chem 5, 3207–3219
December 12, 2019 © 2019 Elsevier Inc.
https://doi.org/10.1016/j.chempr.2019.10.007

Chem

CellPress

Article

Electrostatic Stabilization of Single-Atom Catalysts by Ionic Liquids

Shipeng Ding,[1,7] Yalin Guo,[5,6,7] Max J. Hülsey,[1] Bin Zhang,[1] Hiroyuki Asakura,[2,*] Lingmei Liu,[3] Yu Han,[3] Min Gao,[4,*] Jun-ya Hasegawa,[4] Botao Qiao,[5,*] Tao Zhang,[5,6] and Ning Yan[1,8,*]

SUMMARY

In single-atom catalysts (SACs), the isolated metal atoms on solid support are often charged. Taking advantage of this common feature, we establish ionic liquid-stabilized single-atom catalysts (ILSSACs) employing electrostatic interaction as a general stabilization strategy. While Pt nanoparticles were formed on hydroxyapatite after reaction when unprotected, Pt remained atomically dispersed on ionic liquid-stabilized samples. Density functional theory calculations reveal that the activation energy for the transformation of two isolated Pt atoms to a Pt dimer increases remarkably from 0.11 to 0.72 eV with the protection of [Bmim][BF_4]. The presence of ILs also tunes the electronic state of Pt_1, inducing an order-of-magnitude hydrogenation activity increase. The simple stabilization strategy is easily extended to SACs comprising various metal atom-support combinations. For instance, ILs significantly improved the stability and selectivity of a Pd_1 catalyst for the hydrogenation of acetylene, thus outperforming unprotected SACs.

The Bigger Picture

SACs with maximized atomic efficiency of metal species and unique geometric and electronic structures show remarkable performance in a wide range of chemical reactions. However, the stabilization of SACs depends largely on engineering the support defects or modulating metal-support interactions, which are limited to particular metal-support combinations. Herein, we develop the concept of ionic liquid-stabilized single-atom catalysts (ILSSACs), where an electrical double layer of ILs surrounding supported single-atom species provides electrostatic stabilization against the aggregation of isolated metal atoms. Although electrostatic interaction has been widely applied in the past century for the synthesis of stable colloidal nanoparticles, it has not been systematically applied in the stabilization of SACs. This study, therefore, establishes a general strategy that, in principle, is applicable to enhance the stability of any existing and upcoming SACs.

INTRODUCTION

Single-atom catalysts (SACs) have recently attracted the attention of intense research activities.[1–34] However, the stability of SACs remains an issue as isolated atoms tend to aggregate into thermodynamically more stable nanoparticles (NPs). One approach to enhance the stability of single atoms is to construct defect sites on supports to enhance the binding strength with single atoms.[35] For example, the defects of FeO_x,[1,36] Al_2O_3,[37] $Ni(OH)_2$,[38] and graphene[39,40] strongly anchor atomically dispersed metal atoms. The second strategy is to spatially confine single metal atoms within microporous supports such as zeolites and metal-organic frameworks.[41–44] For instance, atomically dispersed Ti active sites were confined in the framework of two-dimensional zeotypes, showing excellent performance in cyclohexene epoxidation.[43] Stable single-atom catalysts have also been prepared by introducing atoms with lone pairs of electrons, such as N and S, onto the support.[35,45,46] For instance, carbon nitrides (C_3N_4) containing abundant N coordination sites were applied in SAC synthesis.[46,47] These strategies require particular supports and synthetic conditions and therefore, to some extent, lack broad applicability.

Ionic liquids (ILs) have been proven effective in improving the stability of metal NPs. The protective layer introduced by the ILs provides electrostatic protection against aggregation.[48,49] Since the pioneering work by Dupont et al. demonstrating that imidazolium ILs are suitable medium to stabilize Ir NPs,[50] several hundred studies regarding the synthesis and catalytic applications of various NPs in ILs have been reported.[51–53] ILs also found applications in "supported ionic liquid catalysis,"[54] in which the surface of the support is covered by a layer of ILs serving as the medium

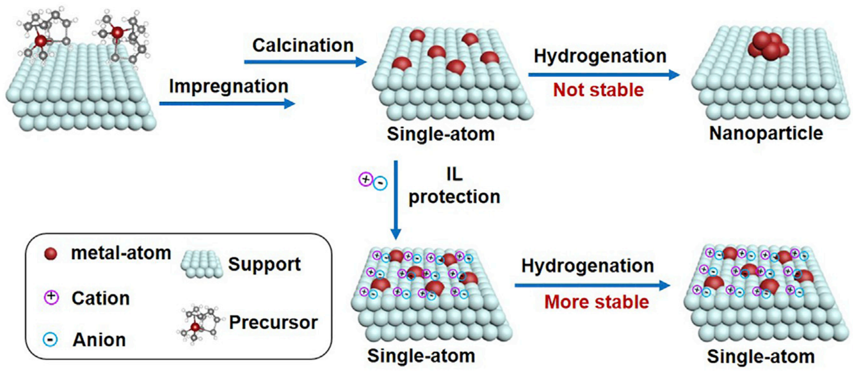

Scheme 1. Schematic Illustration of the Preparation of SACs and the Stabilization by ILs

to immobilize homogeneous catalysts.[54,55] 1,3-dialkylimidazolium ILs, for instance, enhanced the selectivity of Ir single-site catalyst in 1,3-butadiene hydrogenation.[56]

As we are aware, there has been no prior report using ILs to enhance the stability of SACs without compromising activity. Considering the remarkable success of ILs in NP and homogeneous catalysis, we propose that the IL-induced electrostatic stabilization may be a viable strategy to enhance the stability of single-atom catalysts. We also envisage that the electronic modification of isolated metal atoms by charged cation or anion may bring about improved catalytic activity and selectivity. In this proof of concept study, the effect of adding common ILs to single-atom Pt_1 and Pd_1 on several supports was investigated. In the beginning, the ILSSAC $0.2Pt_1$/HAP (hydroxyapatite) was selected as an example to systematically characterize the dispersion state of Pt before and after hydrogenation reaction and quantify the electrostatic stabilization effect of ILs on single-atom Pt using density functional theory (DFT) calculation. Afterward, we extend the strategy to Pt_1 catalysts dispersed on various supports and single-atom Pd_1 catalyst loaded on HAP to prove the general applicability of the strategy.

RESULTS AND DISCUSSION

The Formation of Single-Atom Pt_1/HAP Catalysts

A simple impregnation method was adopted to prepare single-atom Pt_1 catalysts using $PtCODMe_2$ as the precursor and HAP as the support (Scheme 1). $PtCODMe_2$ contains pure organic ligands that are removable under relatively mild conditions, while HAP has a high density of surface OH groups to replace the organic ligands of the precursor.[57] The FTIR spectrum of the prepared sample (Figure S1) did not show C–H vibrations of the COD and Me groups, indicating complete removal of ligands. The obtained catalyst with 0.2 wt % loading was denoted as $0.2Pt_1$/HAP. We employ three ILs bearing 1-n-butyl-3-methylimidazolium [$Bmim^+$] cation, combined with either tetrafluoroborate [BF_4^-], bis(trifluoromethanesulfonyl)imide [Tf_2N^-], or trifluoromethanesulfonate [$CF_3SO_3^-$], all of which belong to non-coordinating anions. The coating of ILs on Pt was facile: first mix $0.2Pt_1$/HAP and ILs (Pt:IL = 1:6) in methanol, followed by solvent evaporation. The IL-modified Pt_1 catalysts were labeled as IL-$0.2Pt_1$/HAP, e.g., $BmimTf_2N$-$0.2Pt_1$/HAP refers to [Bmim][Tf_2N] coated $0.2Pt_1$/HAP catalyst. High angle annular dark-field scanning transmission electron microscopy (HAADF-STEM) confirmed atomic dispersion of Pt on HAP, as separated Pt atoms (circled) were clearly observed as white dots in both $0.2Pt_1$/HAP (Figures 1A and S2) and $BmimTf_2N$-$0.2Pt_1$/HAP (Figures 1B and S3). No NPs were detected. Besides, a shell around the HAP particle was identified in $BmimTf_2N$-$0.2Pt_1$/HAP

[1]Department of Chemical and Biomolecular Engineering, National University of Singapore, 4 Engineering Drive 4, Singapore 117585, Singapore

[2]Department of Molecular Engineering, Graduate School of Engineering, Japan and Elements Strategy Initiative for Catalysts & Batteries (ESICB), Kyoto University, Kyotodaigaku Katsura Nishikyo-ku, Kyoto 615-8510 615-8245, Japan

[3]Advanced Membranes and Porous Materials Center, Physical Sciences and Engineering Division, King Abdullah University of Science and Technology, Thuwal 23955-6900, Saudi Arabia

[4]Institute for Catalysis, Hokkaido University, Sapporo 060-0810, Japan

[5]CAS Key Laboratory of Science and Technology on Applied Catalysis, Dalian Institute of Chemical Physics, Chinese Academy of Sciences, Dalian, 116023, China

[6]University of Chinese Academy of Sciences, Beijing 100049, China

[7]These authors contributed equally

[8]Lead Contact

*Correspondence:
asakura@moleng.kyoto-u.ac.jp (H.A.),
gaomin@cat.hokudai.ac.jp (M.G.),
bqiao@dicp.ac.cn (B.Q.),
ning.yan@nus.edu.sg (N.Y.)

https://doi.org/10.1016/j.chempr.2019.10.007

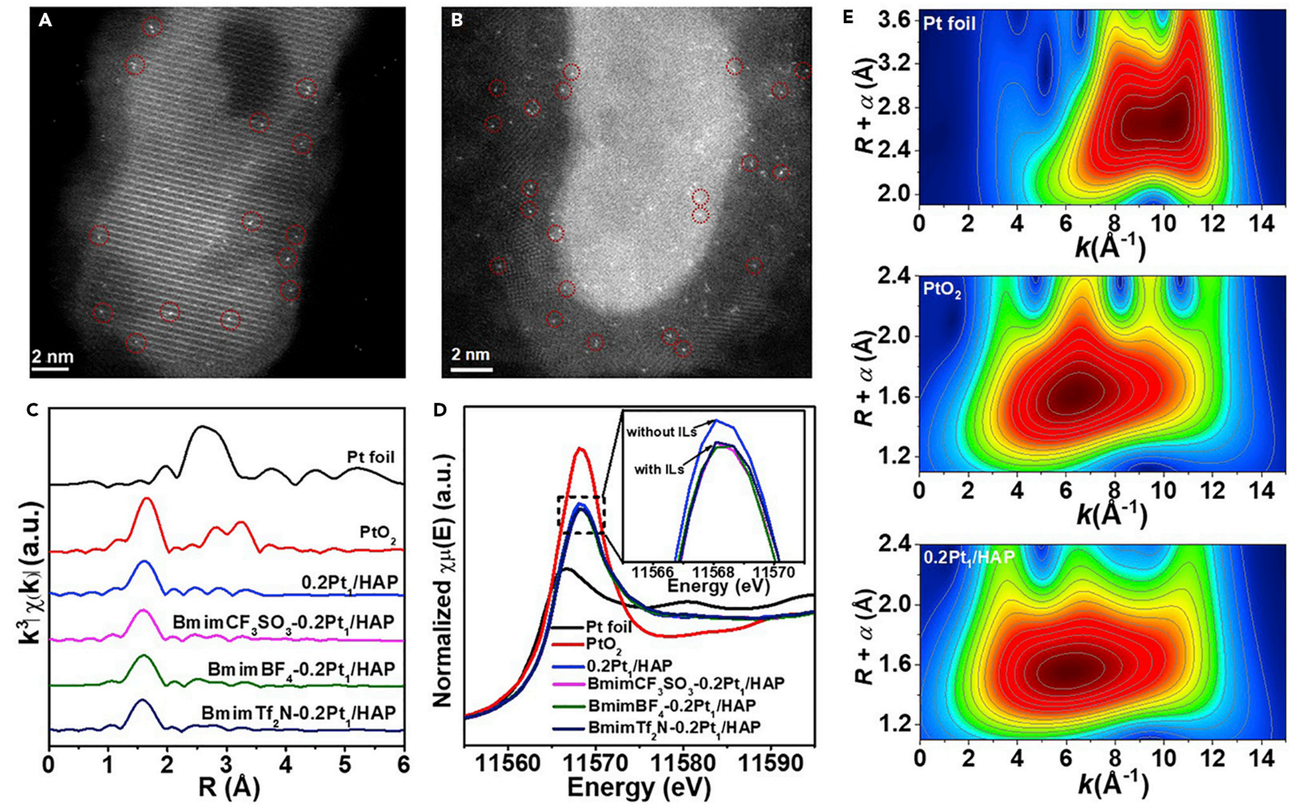

Figure 1. Structural Characterization of Fresh $0.2Pt_1/HAP$ and ILs-0.2Pt/HAP

(A and B) HAADF-STEM images of (A) 0.2 Pt_1/HAP and (B) $BmimTf_2N$-$0.2Pt_1/HAP$.

(C) The k^3-weighted Fourier transform spectra from EXAFS for $0.2Pt_1/HAP$, IL-$0.2Pt_1/HAP$, and standard samples.

(D) The normalized XANES spectra at the Pt L_3-edge for $0.2Pt_1/HAP$, ILs-$0.2Pt_1/HAP$, and standard samples.

(E) Wavelet transfer of the k^3-weighted EXAFS for Pt foil, PtO_2, and 0.2 Pt_1/HAP.

(Figure S3C), likely to be the IL layer on the support. As expected, the X-ray diffraction (XRD) pattern of $0.2Pt_1/HAP$ (Figure S4) was identical to that of HAP, where no peak was assignable to Pt NPs.

The coordination environment and the oxidation state of Pt atoms on HAP were examined by X-ray absorption spectroscopy (XAS). As shown in Figure 1C, the Pt–Pt contribution appeared at around 2.6 Å in the k^3-weighted Fourier transform spectra from extended X-ray absorption fine structure (EXAFS) for Pt foil. However, only one prominent peak centered at 1.6 Å from the Pt-O contribution was identified for $0.2Pt_1/HAP$ and ILs-$0.2Pt_1/HAP$ (Figure 1C). Wavelet transform spectra from EXAFS provide not only radial distance resolution but also resolution in k-space.[58] As shown in the contour plot of Pt foil and PtO_2 (Figure 1E), the intensity maxima at around 10 and 6 Å^{-1} are assigned to Pt–Pt and Pt–O contributions, respectively. For $0.2Pt_1/HAP$ catalyst, only one intensity maximum near 6 Å^{-1} was detected. The wavelet transform spectra of IL-$0.2Pt_1/HAP$ were exhibited in Figure S5. Both Fourier and wavelet transform indicated the dominant existence of single-atom Pt species on HAP. The fitting results of EXAFS are summarized in Figure S6 and Table S1. The coordination number of Pt–O for $0.2Pt_1/HAP$ was 4.1, meaning that each Pt atom coordinates to approximately four oxygen atoms. The modification of $0.2Pt_1/HAP$ with ILs [Bmim][BF_4], [Bmim][Tf_2N], and [Bmim][CF_3SO_3] did not change the coordination number of Pt. The Pt–O bond distance (2.00 Å) of $0.2Pt_1/HAP$ was similar to that of PtO_2 (2.02 Å), implying that the Pt is bound to O in a similar environment to that of PtO_2.

Figure 1D shows the normalized X-ray absorption near edge structure (XANES) results of single-atom Pt catalysts as well as the reference samples Pt foil and PtO_2. The white-line intensity of 0.2Pt_1/HAP was higher than that of Pt foil, suggesting positively charged state of Pt atoms induced by electron transfer from Pt to the support, as commonly seen in SACs. Compared with 0.2Pt_1/HAP, ILs-0.2Pt_1/HAP showed decreased white-line intensity, indicating that the electronic properties of single-atom Pt were slightly tuned. As the oxidation state of active species plays an essential role in catalysis, the reduced charge state hints at a varied catalytic activity. The position of CO adsorption peak in the *in situ* diffuse reflectance infrared Fourier transform spectra (*in situ* DRIFTS) varies according to the oxidation state of Pt and the bonding configuration of CO to Pt.[59] 0.2Pt_1/HAP and ILs-0.2Pt_1/HAP samples only exhibited a narrow and symmetric CO adsorption band peaked at 2,086–2,089 cm^{-1} with full width at half maximum (FWHM) of 21–24 cm^{-1} (Figure S7), assignable to linearly adsorbed CO on positively charged single-atom Pt.[37] Compared with CO adsorption on 0.2Pt_1/HAP (2,089.1 cm^{-1}), a slight red shift was observed for $BmimBF_4$-0.2Pt_1/HAP (2,088.5 cm^{-1}), $BmimTf_2N$-0.2Pt_1/HAP (2,087.1 cm^{-1}), and $BmimCF_3SO_3$-0.2Pt_1/HAP (2,086.6 cm^{-1}), suggesting increased "d" electron back donating to Pt after adding ILs, likely induced by the charge transfer from electron-enriched anions to positively charged Pt_1 species. A negative correlation between turnover frequency (TOF) and oxidation state of Pt was observed (Figure S8), in agreement with an earlier report in which the IL effect on immobilized Ir complex in selective hydrogenation was studied.[56] $BmimCF_3SO_3$-0.2Pt_1/HAP with the lowest oxidation state of Pt showed the highest TOF (Figure 3A).

ILs Enhanced the Stability and Activity of Single-Atom Pt_1/HAP Catalyst in Propylene Hydrogenation

Reducing agents such as H_2 are known to induce the aggregation of noble metals on supports.[60,61] To verify the promotional effect of ILs on the stability of Pt SACs, 0.2Pt_1/HAP and ILs-0.2Pt_1/HAP were tested in propylene hydrogenation at 90°C for 1 h. In the HAADF-STEM image of spent samples, Pt NPs clearly formed on 0.2Pt_1/HAP (Figure 2A). In contrast, atomically dispersed Pt remained to be the only identifiable species on $BmimTf_2N$-0.2Pt_1/HAP (Figures 2B and S9). Fourier transform spectra (Figure 2C) from EXAFS showed that $BmimTf_2N$-0.2Pt_1/HAP displayed a dominant peak of Pt–O at 1.6 Å, however, that of 0.2Pt_1/HAP exhibited a strong Pt–Pt shell at 2.6 Å. Wavelet transform for EXAFS provided the same conclusion (Figure 2E): an intensity maximum near 10 $Å^{-1}$ was resolved for 0.2Pt_1/HAP, indicating the formation of Pt nanoparticle; in contrast, no intensity maximum that can be ascribed to Pt–Pt contribution was observed for $BmimTf_2N$-0.2Pt_1/HAP. For CO adsorption (Figure 2D), IL-coated samples showed a single CO stretching band at around 2,087 cm^{-1} while 0.2Pt_1/HAP exhibited two more peaks at around 2,040 and 1,850 cm^{-1}, which are characteristic for Pt NPs. Similar results were obtained when samples were reduced in H_2 at 90°C for 1 h, i.e., [Bmim][BF_4] and [Bmim][Tf_2N] offered more stabilization effect against the aggregation of single-atom Pt species in comparison to [Bmim][CF_3SO_3] (Figure S10). It should be noted that catalysts treated under propylene hydrogenation conditions were more stable than that reduced in H_2, which could be explained by the stronger adsorption ability of propylene on the catalysts than that of H_2, thus partially blocking the access of H_2 to the catalyst. The HAADF-STEM, EXAFS, and CO DRIFTS results provided compelling evidence that ILs considerably increased the stability of 0.2Pt_1/HAP during hydrogenation reaction. Based on

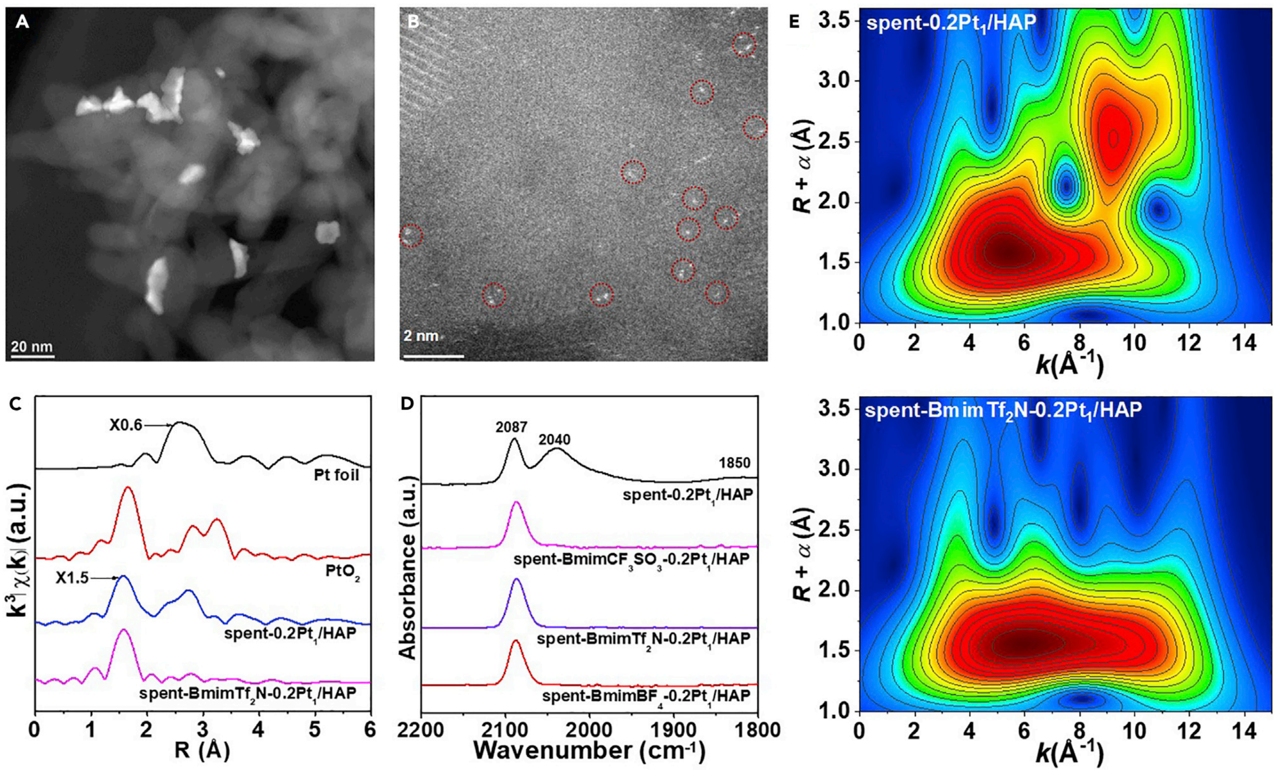

Figure 2. Structural Characterization of 0.2Pt_1/HAP and ILs-0.2Pt/HAP after Propylene Hydrogenation at 90°C for 1 h

(A and B) HAADF-STEM images of (A) 0.2 Pt_1/HAP and (B) $BmimTf_2N$-0.2Pt_1/HAP.

(C) The k^3-weighted Fourier transform spectra from EXAFS for 0.2Pt_1/HAP and $BmimTf_2N$-0.2Pt_1/HAP.

(D) *In situ* FTIR spectra of CO adsorption for 0.2Pt_1/HAP and ILs-0.2Pt_1/HAP catalysts. Pt foil and PtO_2 were used as standard samples.

(E) Wavelet transform of the k^3-weighted EXAFS for 0.2 Pt_1/HAP and $BmimTf_2N$-0.2Pt_1/HAP.

TEM analysis shown earlier, the ILs form a protective layer around single-atom Pt to provide electrostatic stabilization against aggregation.

Further study suggested ILs not only influence the stability of SACs, but also affect the catalytic performance. To ensure all catalysts are stable, we evaluated their activity in propylene hydrogenation at room temperature (Figure 3A). 0.2Pt_1/HAP showed a TOF of 8 h^{-1}, in agreement with earlier reports that SACs are normally not highly active in alkene hydrogenation.[62] In contrast, the TOF increased substantially to 35 h^{-1} for $BmimBF_4$-0.2Pt_1/HAP, 67 h^{-1} for $BmimTf_2N$-0.2Pt_1/HAP, and 81 h^{-1} for $BmimCF_3SO_3$-0.2Pt_1/HAP under the same condition. In the presence of ILs, the single-atom Pt_1 catalyst substantially improved the hydrogenation activity by up to 10 times in the case of $BmimCF_3SO_3$. Both XAS and CO DRIFTS (Figure S11) confirmed that the Pt_1 species were preserved in the spent catalysts. The reaction orders in terms of H_2 and propylene were measured by keeping the reaction in a kinetically limited region with the conversions below 5% (Figure S12).[63,64] For both 0.2Pt_1/HAP and $BmimTf_2N$-0.2Pt_1/HAP, the reaction order was around −0.5 with respect to propylene (Figures 3C and S13A), and 1.1 with respect to H_2 (Figures 3D and S13B). While the reaction orders were identical for the two catalysts, the apparent activation energy was 66 kJ/mol for 0.2Pt_1/HAP and 41 kJ/mol for $BmimTf_2N$-0.2Pt_1/HAP, respectively (Figure 3B), providing insights on why IL-coated catalyst is superior.[65] Using ILs to tune the catalytic properties of metal NPs[66] and an immobilized metal complex[56] through electron-donating effects has been reported, but it has not been previously seen in SACs.

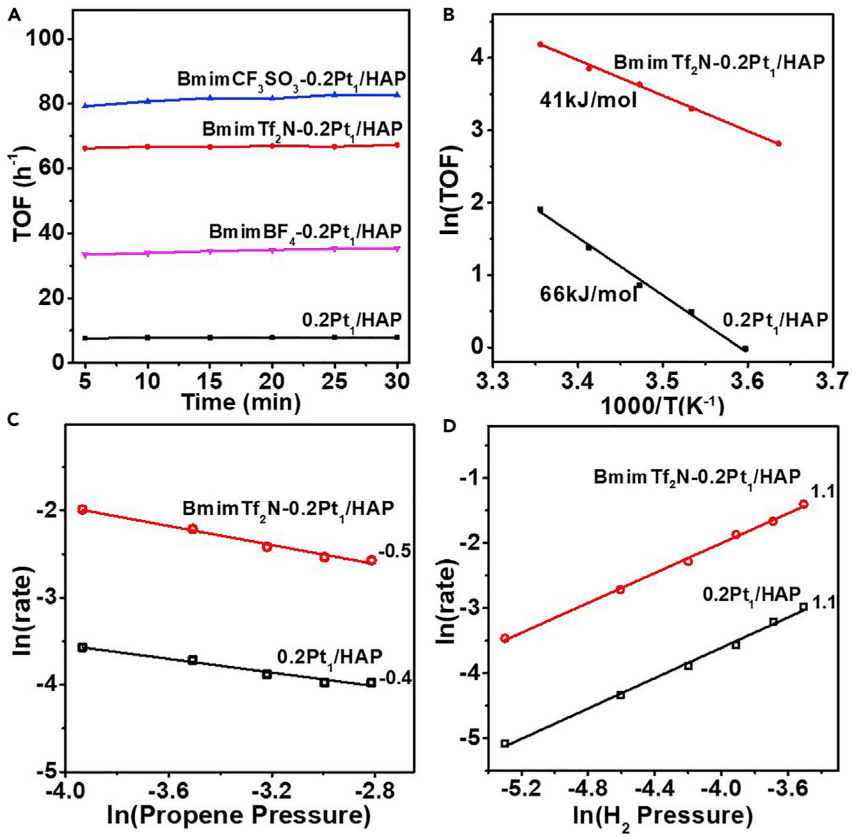

Figure 3. The Effect of ILs on the Catalytic Performance and Kinetic Behavior of $0.2Pt_1/HAP$ during Propylene Hydrogenation

(A) The activity of $0.2Pt_1/HAP$ and ILs-$0.2Pt_1/HAP$. Reaction condition: 3 vol % H_2 and 3 vol % propylene. Flow rate: 30 mL/min, room temperature.

(B) Arrhenius plots of reactions over $0.2Pt_1/HAP$ and $BmimTf_2N$-$0.2Pt_1/HAP$. The reaction temperature ranges from 2°C to 25°C.

(C and D) Propylene (C) and H_2 reaction orders measured at 25°C over $0.2Pt_1/HAP$ and $BmimTf_2N$-$0.2Pt_1/HAP$ (D).

DFT Simulation to Quantify the Electrostatic Stabilization Effect of ILs

DFT calculations were performed to clarify and quantify the role of ILs in preventing Pt atoms from aggregation. The computational details are shown in the Supplemental Information. [Bmim][BF_4] was selected instead of the other two ILs bearing larger anions to reduce the computational cost. We first consider the formation process of a Pt dimer (Pt_2@HAP) from two isolated Pt_1 species on HAP without ILs. As shown in Figure 4, the Pt_1 species prefer to adsorb on the oxygen atom of a HAP surface with a Pt–O bond length of 1.99 Å. In Pt_2@HAP, the Pt–Pt bond is 2.44 Å, slightly longer than that of the isolated Pt dimer in a vacuum (2.36 Å), indicating that Pt–Pt interaction is weakened by HAP. The energy profile shows that the process from two Pt atoms to the Pt dimer is highly exothermic. The Pt dimer is more stable than two Pt atoms on HAP by ca. 2 eV. Moreover, the energy barrier for the transformation of 2 Pt_1 species into a Pt_2 dimer is remarkably low (0.11 eV), explaining why Pt single atoms are not stable on HAP. In the transition state, one Pt–O bond is elongated to 2.21 Å, whereas two Pt atoms come closer to form a Pt–Pt bond.

When a [Bmim]/[BF_4] couple is introduced, the [BF_4^-] adopts a bridge mode to interact with both Pt_1 species. To form a Pt dimer, one must weaken both Pt–BF_4^-

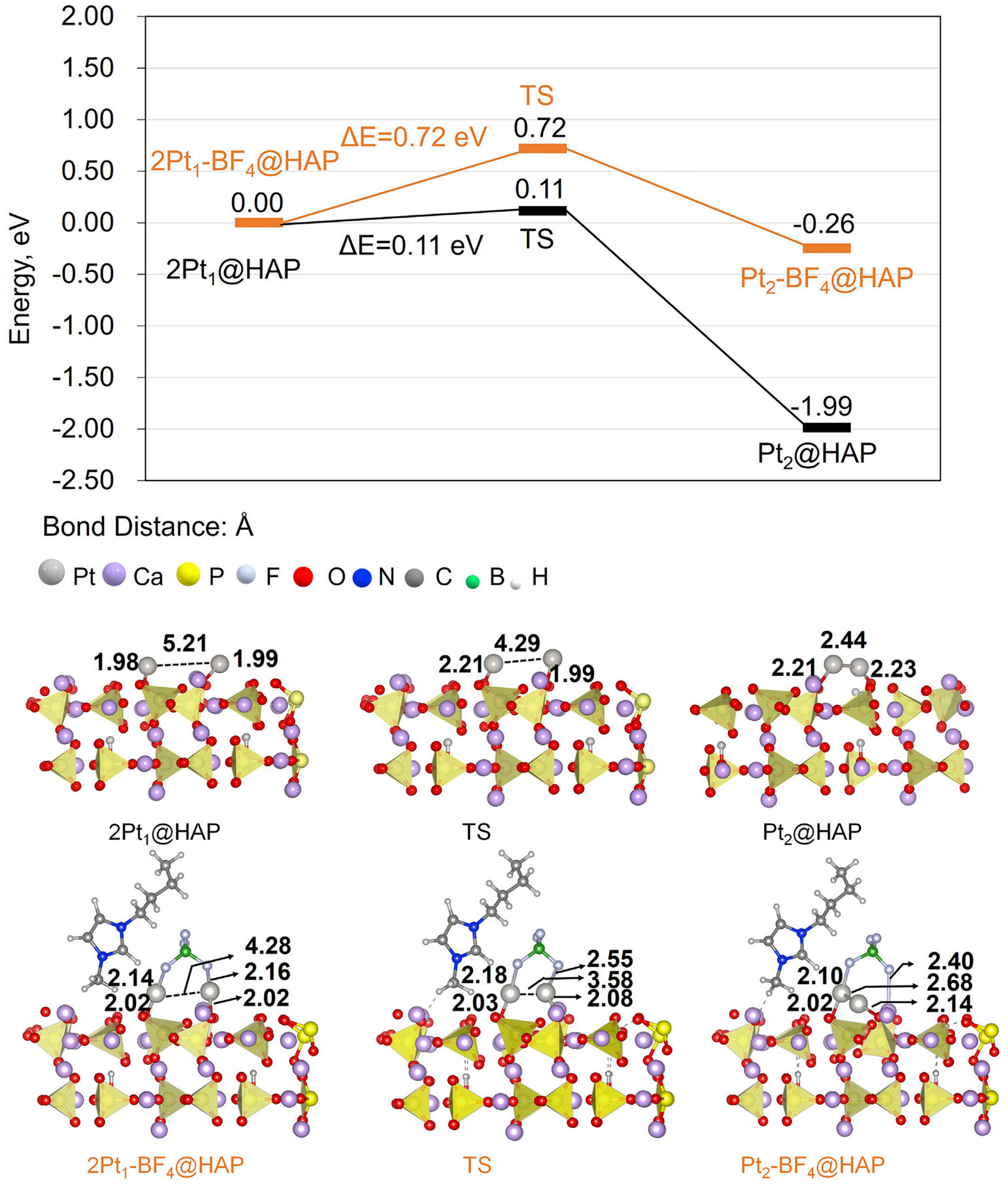

Figure 4. The Energy Profiles of the Dimerization Process for Two Pt Atoms on HAP Surface Without (Black) and With (Orange) [Bmim][BF$_4$]

The corresponding structures are shown below the energy profiles. The indication of colors for each atom is shown at the top of the structures. TS stands for the transition state.

interactions and Pt–O bonds with an activation barrier of 0.72 eV, 6 times higher than the one without [Bmim][BF_4]. The [BF_4^-] keeps strong interaction with both Pt atoms in the transition state, and still bonds to one Pt atom after the dimer formation. Influenced by [BF_4^-] in the close proximity, the bond length of Pt–Pt in Pt_2@HAP increases to 2.68 Å, which narrows down the energy difference between $2Pt_1$-BF_4@HAP and Pt_2-BF_4@HAP to 0.25 eV. These results provide molecular-level insights on how ILs protect the isolated Pt atoms: the anion plays a dominant role in stabilization and electronic modulation by directly interacting with Pt_1 species on the support, while the cation stays in the outer shell balancing the charge and possibly provides additional steric stabilization.[61]

The Generalization of ILSSAC for Different Supports and Transition Metals

To confirm that ILs stabilization is a general method to stabilize SACs, [Bmim][Tf_2N] was coated on single-atom Pt_1 species that were dispersed on various supports including CeO_2, rutile TiO_2, and monoclinic ZrO_2. As shown in Figure 5A, after reduction at 200°C for 1 h in H_2, all the ionic liquid-stabilized single-atom Pt_1 catalysts displayed a dominant CO adsorption peak at above 2,080 cm^{-1}, indicating the atomic dispersion of Pt after reduction under harsh conditions; however, single-atom Pt_1 catalysts without adding ILs exhibited a strong peak between 2,053 and 2,037 cm^{-1}, and a broad peak near 1,800 cm^{-1}, which were assigned to CO adsorption on Pt nanoparticles. As such, ILs stabilization of single-atom Pt_1 against aggregation is easily extendable to a range of common metal oxide supports. The reduction temperature was further increased from 200°C to 240°C and 280°C. The single-atom identity of Pt was fully preserved at 240°C, while a peak ascribed to CO adsorption on Pt nanoparticles was identified on $BmimTf_2N$-$0.2Pt_1/ZrO_2$ reduced at 280°C (Figure S14), indicating $BmimTf_2N$ is able to stabilize Pt single atoms up to around 240°C. In case even higher temperature tolerance under a strong reduction condition is needed, the use of more stable inorganic salts to provide electrostatic interaction may be required.

We also explored ILSSAC beyond Pt. A highly stable, active, and selective Pd_1/HAP SAC for semi-hydrogenation of acetylene using IL stabilization strategy was developed. Semi-hydrogenation of trace acetylene in a gas feed containing excess of ethylene is an industrially important reaction in the purification of ethylene feed gas for polyethylene production.[67–70] Supported Pd catalysts are commonly used in industrial scale due to their superior activity.[71] However, significant quantities of ethylene in the feedstock are also hydrogenated, significantly lowering the selectivity and atom economy.[72] The long-term stability is another issue. It was recently found that supported Pd SACs[9,73] or single-atom alloy (SAS) catalysts[74–76] are highly selective to this reaction, but suffer from the relatively lower activity (e.g., acetylene total conversion at temperature >180°C)[9] and lower atomic efficiency.[74–76]

HAP-supported Pd SAC was prepared by a strong electrostatic adsorption method[77] and was denoted as Pd_1/HAP. [Bmim][BF_4]-modified Pd_1/HAP was denoted as $BmimBF_4$-Pd_1/HAP. As shown in Figure S15, the catalytic performance test in semi-hydrogenation of acetylene in excess ethylene reveals that Pd_1/HAP (IL free) has a relatively higher activity compared with previously reported Pd SACs on which a total acetylene conversion was achieved at 140°C with a relatively higher ethylene selectivity. After reduction at 100°C in H_2, the $0.02Pd_1$/HAP without ILs showed a much-increased activity but dramatically decreased selectivity, suggesting that Pd single atoms have sintered into Pd NPs upon post-reduction treatment. This was evidenced by STEM images where small Pd NPs were observed (Figure 5D). On the contrary, after reduction, the $BmimBF_4$-Pd_1/HAP sample exhibits increased activity

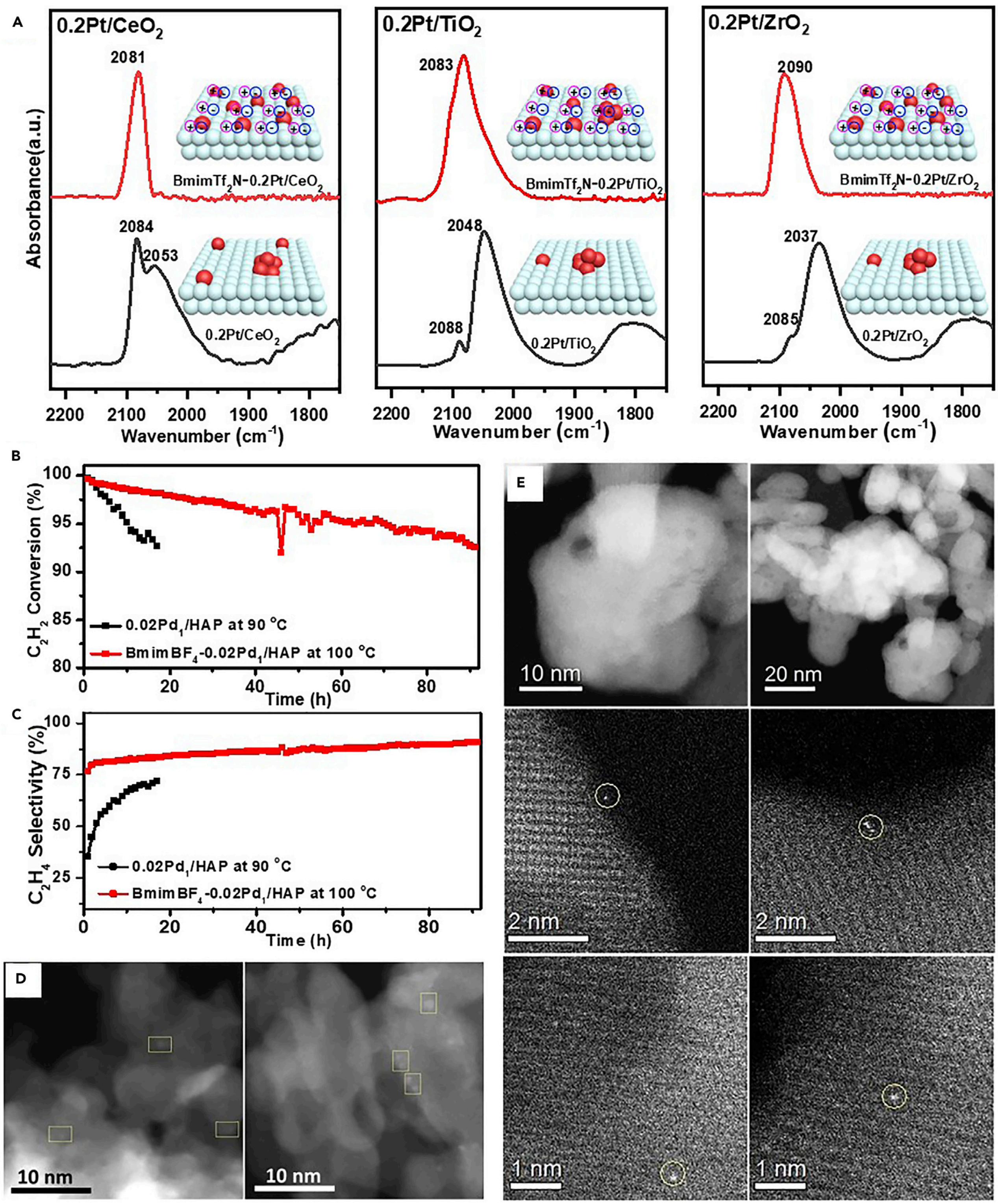

Figure 5. ILs Increased the Stability of a Range of Single-Atom Pt_1 and Pd_1 Catalysts

(A) *In situ* DRIFTS of CO adsorption on SACs and ILSSAC Pt catalysts after reduction at 200°C in 5% H_2/N_2 for 1 h.

(B and C) The acetylene conversion (B) and (C) ethylene selectivity over $0.02Pd_1/HAP$ and $BmimBF_4$-$0.02_1Pd/HAP$ catalysts at 90 and 100°C, respectively. The reaction temperature for each catalyst was set at the point when the catalyst just starts to provide full conversion of acetylene in the initial stage.

(D) The TEM images of $0.02Pd_1/HAP$ reduced by 10% H_2/He at 100°C for 0.5 h.

(E) HAADF-STEM images of $BmimBF_4$-$0.02Pd_1/HAP$ after 90 h acetylene hydrogenation.

and selectivity, demonstrating that the nature of atomic dispersion was retained. The durability of this catalyst was also examined by a long-term reaction test at 100°C (Figures 5B and 5C). It shows that over 90 h on-stream test the acetylene conversion only dropped to 92%, with high ethylene selectivity of >75%. Aberration-corrected HAADF-STEM images of the post-reaction catalyst reveal that no sintering of the single Pd atoms was observed (Figure 5E). Comparatively, $0.02Pd_1$/HAP without [Bmim][BF_4] showed much lower selectivity and durability and the conversion dropped to 92% rapidly within 17 h. It turns out that $BmimBF_4$-Pd_1/HAP exhibited not only superior durability but also much higher selectivity at similar condition than Pd_1/HAP. Thermogravimetry and differential thermal analysis (TG-DTA) was performed on the spent Pd/HAP catalyst (without ionic liquid coating). A clear weight loss was observed before 600°C, suggesting the formation of oligomers as by-products, which might be the reason for the slow deactivation (Figure S16).

In summary, we have established a simple and general method to stabilize SACs by IL-coating. ILs provide sufficient protection to isolated metal atoms such as Pt and Pd on HAP or other supports, thus significantly increasing the kinetic barrier for the formation of metal-metal bonds on the surface. The presence of ILs also makes the atom aggregation thermodynamically less favorable. Meanwhile, ILs tune the electronic state of Pt/Pd atoms to improve their catalytic stability and activity in hydrogenation reactions, including industrially important semi-hydrogenation of trace acetylene in a gas feed containing excess of ethylene. Considering that the physicochemical properties of ILs can be easily and finely tuned by the rational control of cations and anions, it is likely that the electrostatic stabilization becomes a simple and general strategy to enhance the stability of a broad range of SACs already reported in the literature or under developments in various labs.

EXPERIMENTAL PROCEDURES

The Experimental Procedures are provided in the Supplemental Information.

SUPPLEMENTAL INFORMATION

Supplemental Information can be found online at https://doi.org/10.1016/j.chempr.2019.10.007.

ACKNOWLEDGMENTS

This work has been supported by the National University of Singapore Flagship Green Energy Program (#R-279-000-553-646 and R-279-000-553-731). The computations were partly performed at the Research Center for Computational Science, Okazaki, Japan, and partly supported by Grant-in-Aid for Young Scientists (B) (17K1442907) in Japan.

AUTHOR CONTRIBUTIONS

N.Y. conceived and supervised the project. S.D. carried out the catalyst synthesis, catalytic performance test, stability evaluation, and kinetic study and conducted some characterizations. S.D., N.Y., M.H., and B.Z. analyzed the data. L.L. and Y.H. carried out the HAADF-STEM characterizations. H.A. carried out the XAS measurements and analysis. M.G. and J.H. conducted the DFT calculation. S.D. and N.Y. wrote the paper. Y.G., B.Q., and T.Z. prepared the Pd/HAP catalyst, performed the HADDF-STEM and acetylene hydrogenation measurement, and wrote the Pd/HAP section. All authors contributed to project discussions and modified the manuscript.

DECLARATION OF INTERESTS

The authors declare no competing interests.

Received: July 28, 2019
Revised: August 28, 2019
Accepted: October 11, 2019
Published: November 4, 2019

REFERENCES AND NOTES

1. Qiao, B., Wang, A., Yang, X., Allard, L.F., Jiang, Z., Cui, Y., Liu, J., Li, J., and Zhang, T. (2011). Single-atom catalysis of CO oxidation using Pt_1/FeOx. Nat. Chem. *3*, 634–641.

2. Thomas, J.M., Saghi, Z., and Gai, P.L. (2011). Can a single atom serve as the active site in some heterogeneous catalysts? Top. Catal. *54*, 588–594.

3. Flytzani-Stephanopoulos, M., and Gates, B.C. (2012). Atomically dispersed supported metal catalysts. Annu. Rev. Chem. Biomol. Eng. *3*, 545–574.

4. Liu, J. (2017). Catalysis by supported single metal atoms. ACS Catal. *7*, 34–59.

5. Lin, L., Zhou, W., Gao, R., Yao, S., Zhang, X., Xu, W., Zheng, S., Jiang, Z., Yu, Q., Li, Y.W., et al. (2017). Low-temperature hydrogen production from water and methanol using Pt/alpha-MoC catalysts. Nature *544*, 80–83.

6. Jeong, H., Lee, G., Kim, B.S., Bae, J., Han, J.W., and Lee, H. (2018). Fully dispersed Rh ensemble catalyst to enhance low-temperature activity. J. Am. Chem. Soc. *140*, 9558–9565.

7. Chen, Z., Vorobyeva, E., Mitchell, S., Fako, E., López, N., Collins, S.M., Leary, R.K., Midgley, P.A., Hauert, R., and Pérez-Ramírez, J. (2018). Single-atom heterogeneous catalysts based on distinct carbon nitride scaffolds. Natl. Sci. Rev. *5*, 642–652.

8. Zhang, L., Doyle-Davis, K., and Sun, X. (2019). Pt-Based electrocatalysts with high atom utilization efficiency: from nanostructures to single atoms. Energy Environ. Sci. *12*, 492–517.

9. Huang, F., Deng, Y., Chen, Y., Cai, X., Peng, M., Jia, Z., Ren, P., Xiao, D., Wen, X., Wang, N., et al. (2018). Atomically dispersed Pd on nanodiamond/graphene hybrid for selective hydrogenation of acetylene. J. Am. Chem. Soc. *140*, 13142–13146.

10. Li, T., Liu, F., Tang, Y., Li, L., Miao, S., Su, Y., Zhang, J., Huang, J., Sun, H., Haruta, M., et al. (2018). Maximizing the number of interfacial sites in single-atom catalysts for the highly selective, solvent-free oxidation of primary alcohols. Angew. Chem. Int. Ed. *57*, 7795–7799.

11. Millet, M.M., Algara-Siller, G., Wrabetz, S., Mazheika, A., Girgsdies, F., Teschner, D., Seitz, F., Tarasov, A., Levchenko, S.V., Schlögl, R., et al. (2019). Ni single atom catalysts for CO_2 activation. J. Am. Chem. Soc. *141*, 2451–2461.

12. Zhang, X., Sun, Z., Wang, B., Tang, Y., Nguyen, L., Li, Y., and Tao, F.F. (2018). C-C coupling on single-atom-based heterogeneous catalyst. J. Am. Chem. Soc. *140*, 954–962.

13. Liu, J., Lucci, F.R., Yang, M., Lee, S., Marcinkowski, M.D., Therrien, A.J., Williams, C.T., Sykes, E.C., and Flytzani-Stephanopoulos, M. (2016). Tackling CO poisoning with single-atom alloy catalysts. J. Am. Chem. Soc. *138*, 6396–6399.

14. Ling, C., Niu, X., Li, Q., Du, A., and Wang, J. (2018). Metal-free single atom catalyst for N_2 fixation driven by visible light. J. Am. Chem. Soc. *140*, 14161–14168.

15. Zhao, D., Chen, Z., Yang, W., Liu, S., Zhang, X., Yu, Y., Cheong, W.C., Zheng, L., Ren, F., Ying, G., et al. (2019). MXene (Ti_3C_2) vacancy-confined single-atom catalyst for efficient functionalization of CO_2. J. Am. Chem. Soc. *141*, 4086–4093.

16. Nie, L., Mei, D., Xiong, H., Peng, B., Ren, Z., Hernandez, X.I.P., DeLaRiva, A., Wang, M., Engelhard, M.H., Kovarik, L., et al. (2017). Activation of surface lattice oxygen in single-atom Pt/CeO_2 for low-temperature CO oxidation. Science *358*, 1419–1423.

17. Pereira-Hernández, X.I., DelaRiva, A., Muravev, V., Kunwar, D., Xiong, H., Sudduth, B., Engelhard, M., Kovarik, L., Hensen, E.J.M., Wang, Y., et al. (2019). Tuning Pt-CeO_2 interactions by high-temperature vapor-phase synthesis for improved reducibility of lattice oxygen. Nat. Commun. *10*, 1358.

18. Lu, Y., Wang, J., Yu, L., Kovarik, L., Zhang, X., Hoffman, A.S., Gallo, A., Bare, S.R., Sokaras, D., Kroll, T., et al. (2019). Identification of the active complex for CO oxidation over single-atom Ir-on-$MgAl_2O_4$ catalysts. Nat. Catal. *2*, 149–156.

19. Liu, P., Zhao, Y., Qin, R., Mo, S., Chen, G., Gu, L., Chevrier, D.M., Zhang, P., Guo, Q., Zang, D., et al. (2016). Photochemical route for synthesizing atomically dispersed palladium catalysts. Science *352*, 797–801.

20. Sun, G., Zhao, Z.J., Mu, R., Zha, S., Li, L., Chen, S., Zang, K., Luo, J., Li, Z., Purdy, S.C., et al. (2018). Breaking the scaling relationship via thermally stable Pt/Cu single atom alloys for catalytic dehydrogenation. Nat. Commun. *9*, 4454.

21. Zhao, L., Zhang, Y., Huang, L.B., Liu, X.Z., Zhang, Q.H., He, C., Wu, Z.Y., Zhang, L.J., Wu, J., Yang, W., et al. (2019). Cascade anchoring strategy for general mass production of high-loading single-atomic metal-nitrogen catalysts. Nat. Commun. *10*, 1278.

22. Mitchell, S., Vorobyeva, E., and Pérez-Ramírez, J. (2018). The multifaceted reactivity of single-atom heterogeneous catalysts. Angew. Chem. Int. Ed. *57*, 15316–15329.

23. Shao, X., Yang, X., Xu, J., Liu, S., Miao, S., Liu, X., Su, X., Duan, H., Huang, Y., and Zhang, T. (2019). Iridium single-atom catalyst performing a quasi-homogeneous hydrogenation transformation of CO_2 to formate. Chem *5*, 693–705.

24. Tao, H., Choi, C., Ding, L.-X., Jiang, Z., Han, Z., Jia, M., Fan, Q., Gao, Y., Wang, H., Robertson, A.W., et al. (2019). Nitrogen fixation by Ru single-atom electrocatalytic reduction. Chem *5*, 204–214.

25. Cui, X., Li, H., Wang, Y., Hu, Y., Hua, L., Li, H., Han, X., Liu, Q., Yang, F., He, L., et al. (2018). Room-temperature methane conversion by graphene-confined single iron atoms. Chem *4*, 1902–1910.

26. Wang, X., Li, Z., Qu, Y., Yuan, T., Wang, W., Wu, Y., and Li, Y. (2019). Review of metal catalysts for oxygen reduction reaction: from nanoscale engineering to atomic design. Chem *5*, 1486–1511.

27. Jiao, L., and Jiang, H.-L. (2019). Metal-organic-framework-based single-atom catalysts for energy applications. Chem *5*, 786–804.

28. Zhang, L., Jia, Y., Gao, G., Yan, X., Chen, N., Chen, J., Soo, M.T., Wood, B., Yang, D., Du, A., et al. (2018). Graphene defects trap atomic Ni species for hydrogen and oxygen evolution reactions. Chem *4*, 285–297.

29. Jiang, K., Siahrostami, S., Akey, A.J., Li, Y., Lu, Z., Lattimer, J., Hu, Y., Stokes, C., Gangishetty, M., Chen, G., et al. (2017). Transition-metal single atoms in a graphene shell as active centers for highly efficient artificial photosynthesis. Chem *3*, 950–960.

30. Liu, G., Robertson, A.W., Li, M.M., Kuo, W.C.H., Darby, M.T., Muhieddine, M.H., Lin, Y.C., Suenaga, K., Stamatakis, M., Warner, J.H., et al. (2017). MoS_2 monolayer catalyst doped with isolated Co atoms for the hydrodeoxygenation reaction. Nat. Chem. *9*, 810–816.

31. Duan, H., Dong, J., Gu, X., Peng, Y.K., Chen, W., Issariyakul, T., Myers, W.K., Li, M.J., Yi, N., Kilpatrick, A.F.R., et al. (2017). Hydrodeoxygenation of water-insoluble bio-oil to alkanes using a highly dispersed Pd-Mo catalyst. Nat. Commun. *8*, 591.

32. Gates, B.C., Flytzani-Stephanopoulos, M., Dixon, D.A., and Katz, A. (2017). Atomically dispersed supported metal catalysts: perspectives and suggestions for future research. Catal. Sci. Technol. *7*, 4259–4275.

33. Su, Y.-Q., Wang, Y., Liu, J.-X., Filot, I.A.W., Alexopoulos, K., Zhang, L., Muravev, V., Zijlstra, B., Vlachos, D.G., and Hensen, E.J.M. (2019). Theoretical approach to predict the stability of

supported single-atom catalysts. ACS Catal. *9*, 3289–3297.

34. Alexopoulos, K., Wang, Y., and Vlachos, D.G. (2019). First-principles kinetic and spectroscopic insights into single-atom catalysis. ACS Catal. *9*, 5002–5010.

35. Chen, Y., Ji, S., Chen, C., Peng, Q., Wang, D., and Li, Y. (2018). Single-atom catalysts: synthetic strategies and electrochemical applications. Joule *2*, 1242–1264.

36. Cao, L., Liu, W., Luo, Q., Yin, R., Wang, B., Weissenrieder, J., Soldemo, M., Yan, H., Lin, Y., Sun, Z., et al. (2019). Atomically dispersed iron hydroxide anchored on Pt for preferential oxidation of CO in H_2. Nature *565*, 631–635.

37. Zhang, Z., Zhu, Y., Asakura, H., Zhang, B., Zhang, J., Zhou, M., Han, Y., Tanaka, T., Wang, A., Zhang, T., et al. (2017). Thermally stable single atom Pt/m-Al_2O_3 for selective hydrogenation and CO oxidation. Nat. Commun. *8*, 16100.

38. Zhang, J., Wu, X., Cheong, W.C., Chen, W., Lin, R., Li, J., Zheng, L., Yan, W., Gu, L., Chen, C., et al. (2018). Cation vacancy stabilization of single-atomic-site Pt_1/Ni(OH)x catalyst for diboration of alkynes and alkenes. Nat. Commun. *9*, 1002.

39. Yan, H., Lin, Y., Wu, H., Zhang, W., Sun, Z., Cheng, H., Liu, W., Wang, C., Li, J., Huang, X., et al. (2017). Bottom-up precise synthesis of stable platinum dimers on graphene. Nat. Commun. *8*, 1070.

40. Yan, H., Cheng, H., Yi, H., Lin, Y., Yao, T., Wang, C., Li, J., Wei, S., and Lu, J. (2015). Single-atom Pd1/graphene catalyst achieved by atomic layer deposition: remarkable performance in selective hydrogenation of 1,3-butadiene. J. Am. Chem. Soc. *137*, 10484–10487.

41. Liu, L., Díaz, U., Arenal, R., Agostini, G., Concepción, P., and Corma, A. (2017). Generation of subnanometric platinum with high stability during transformation of a 2D zeolite into 3D. Nat. Mater. *16*, 132–138.

42. He, T., Chen, S., Ni, B., Gong, Y., Wu, Z., Song, L., Gu, L., Hu, W., and Wang, X. (2018). Zirconium-porphyrin-based metal-organic framework hollow nanotubes for immobilization of noble-metal single atoms. Angew. Chem. Int. Ed. *57*, 3493–3498.

43. Grosso-Giordano, N.A., Hoffman, A.S., Boubnov, A., Small, D.W., Bare, S.R., Zones, S.I., and Katz, A. (2019). Dynamic reorganization and confinement of Ti(IV) active sites controls olefin epoxidation catalysis on two-dimensional zeotypes. J. Am. Chem. Soc. *141*, 7090–7106.

44. Grosso-Giordano, N.A., Schroeder, C., Okrut, A., Solovyov, A., Schöttle, C., Chassé, W., Marinković, N., Koller, H., Zones, S.I., and Katz, A. (2018). Outer-sphere control of catalysis on surfaces: a comparative study of Ti(IV) single-sites grafted on amorphous versus crystalline silicates for alkene epoxidation. J. Am. Chem. Soc. *140*, 4956–4960.

45. Li, H., Wang, L., Dai, Y., Pu, Z., Lao, Z., Chen, Y., Wang, M., Zheng, X., Zhu, J., Zhang, W., et al. (2018). Synergetic interaction between neighbouring platinum monomers in CO_2 hydrogenation. Nat. Nanotechnol. *13*, 411–417.

46. Yang, J., Chen, B., Liu, X., Liu, W., Li, Z., Dong, J., Chen, W., Yan, W., Yao, T., Duan, X., et al. (2018). Efficient and robust hydrogen evolution: phosphorus nitride imide nanotubes as supports for anchoring single ruthenium sites. Angew. Chem. Int. Ed. *57*, 9495–9500.

47. Chen, Z., Vorobyeva, E., Mitchell, S., Fako, E., Ortuño, M.A., López, N., Collins, S.M., Midgley, P.A., Richard, S., Vilé, G., et al. (2018). A heterogeneous single-atom palladium catalyst surpassing homogeneous systems for Suzuki coupling. Nat. Nanotechnol. *13*, 702–707.

48. Dupont, J., and Scholten, J.D. (2010). On the structural and surface properties of transition-metal nanoparticles in ionic liquids. Chem. Soc. Rev. *39*, 1780–1804.

49. Yan, N., Xiao, C., and Kou, Y. (2010). Transition metal nanoparticle catalysis in green solvents. Coord. Chem. Rev. *254*, 1179–1218.

50. Dupont, J., Fonseca, G.S., Umpierre, A.P., Fichtner, P.F.P., and Teixeira, S.R. (2002). Transition-metal nanoparticles in imidazolium ionic liquids: recycable catalysts for biphasic hydrogenation reactions. J. Am. Chem. Soc. *124*, 4228–4229.

51. Chun, Y.S., Shin, J.Y., Song, C.E., and Lee, S.G. (2008). Palladium nanoparticles supported onto ionic carbon nanotubes as robust recyclable catalysts in an ionic liquid. Chem. Commun. (Camb.) *8*, 942–944.

52. Zhang, H., and Cui, H. (2009). Synthesis and characterization of functionalized ionic liquid-stabilized metal (gold and platinum) nanoparticles and metal nanoparticle/carbon nanotube hybrids. Langmuir *25*, 2604–2612.

53. Pensado, A.S., and Pádua, A.A. (2011). Solvation and stabilization of metallic nanoparticles in ionic liquids. Angew. Chem. Int. Ed. *50*, 8683–8687.

54. Mehnert, C.P., Cook, R.A., Dispenziere, N.C., and Afeworki, M. (2002). Supported ionic liquid catalysis–a new concept for homogeneous hydroformylation catalysis. J. Am. Chem. Soc. *124*, 12932–12933.

55. Babucci, M., Fang, C.Y., Perez-Aguilar, J.E., Hoffman, A.S., Boubnov, A., Guan, E., Bare, S.R., Gates, B.C., and Uzun, A. (2019). Controlling catalytic activity and selectivity for partial hydrogenation by tuning the environment around active sites in iridium complexes bonded to supports. Chem. Sci. *10*, 2623–2632.

56. Babucci, M., Fang, C.-Y., Hoffman, A.S., Bare, S.R., Gates, B.C., and Uzun, A. (2017). Tuning the selectivity of single-site supported metal catalysts with ionic liquids. ACS Catal. *7*, 6969–6972.

57. Hoffman, A.S., Fang, C.Y., and Gates, B.C. (2016). Homogeneity of surface sites in supported single-site metal catalysts: assessment with band widths of metal carbonyl infrared spectra. J. Phys. Chem. Lett. *7*, 3854–3860.

58. Funke, H., Scheinost, A.C., and Chukalina, M. (2005). Wavelet analysis of extended x-ray absorption fine structure data. Phys. Rev. B *71*, 094110.

59. DeRita, L., Dai, S., Lopez-Zepeda, K., Pham, N., Graham, G.W., Pan, X., and Christopher, P. (2017). Catalyst architecture for stable single atom dispersion enables site-specific spectroscopic and reactivity measurements of CO adsorbed to Pt Atoms, oxidized Pt clusters, and metallic Pt clusters on TiO_2. J. Am. Chem. Soc. *139*, 14150–14165.

60. Serna, P., Yardimci, D., Kistler, J.D., and Gates, B.C. (2014). Formation of supported rhodium clusters from mononuclear rhodium complexes controlled by the support and ligands on rhodium. Phys. Chem. Chem. Phys. *16*, 1262–1270.

61. Schöttle, C., Guan, E., Okrut, A., Grosso-Giordano, N.A., Palermo, A., Solovyov, A., Gates, B.C., and Katz, A. (2019). Bulky calixarene ligands stabilize supported iridium pair-site catalysts. J. Am. Chem. Soc. *141*, 4010–4015.

62. Rossell, M.D., Caparrós, F.J., Angurell, I., Muller, G., Llorca, J., Seco, M., and Rossell, O. (2016). Magnetite-supported palladium single-atoms do not catalyse the hydrogenation of alkenes but small clusters do. Catal. Sci. Technol. *6*, 4081–4085.

63. Mears, D.E. (1971). Tests for transport limitations in experimental catalytic reactors. Ind. Eng. Chem. Proc. Des. Dev. *10*, 541–547.

64. Chambers, P.R., and Boudart, M. (1966). Lack of dependence of conversion on flow rate in catalytic studies. J. Catal. *6*, 141–145.

65. Zhou, X., Shen, Q., Yuan, K., Yang, W., Chen, Q., Geng, Z., Zhang, J., Shao, X., Chen, W., Xu, G., et al. (2018). Unraveling charge state of supported Au single-atoms during CO oxidation. J. Am. Chem. Soc. *140*, 554–557.

66. Jalal, A., and Uzun, A. (2017). An exceptional selectivity for partial hydrogenation on a supported nickel catalyst coated with [BMIM] [BF_4]. J. Catal. *350*, 86–96.

67. McGown, W.T., Kemball, C., Whan, D.A., and Scurrell, M.S. (1977). Hydrogenation of acetylene in excess ethylene on an alumina supported palladium catalyst in a static system. J. Chem. Soc. Faraday Trans. *1*, 632–647.

68. Shi, C., Hoisington, R., and Jang, B.W.-L. (2007). Promotion effects of air and H2 nonthermal plasmas on TiO2 supported Pd and Pd−Ag catalysts for selective hydrogenation of acetylene. Ind. Eng. Chem. Res. *46*, 4390–4395.

69. Osswald, J., Kovnir, K., Armbruster, M., Giedigkeit, R., Jentoft, R., Wild, U., Grin, Y., and Schlogl, R. (2008). Palladium–gallium intermetallic compounds for the selective hydrogenation of acetylene part II: surface characterization and catalytic performance. J. Catal. *258*, 219–227.

70. Rahimpour, M.R., Dehghani, O., Gholipour, M.R., Shokrollahi Yancheshmeh, M.S., Seifzadeh Haghighi, S., and Shariati, A. (2012). A novel configuration for Pd/Ag/α-Al_2O_3 catalyst regeneration in the acetylene hydrogenation reactor of a multi feed cracker. Chem. Eng. J. *198–199*, 491–502.

71. Yan, H., Lv, H., Yi, H., Liu, W., Xia, Y., Huang, X., Huang, W., Wei, S., Wu, X., and Lu, J. (2018). Understanding the underlying mechanism of improved selectivity in Pd1 single-atom catalyzed hydrogenation reaction. J. Catal. *366*, 70–79.

72. Zhou, S., Shang, L., Zhao, Y., Shi, R., Waterhouse, G.I.N., Huang, Y.C., Zheng, L., and Zhang, T. (2019). Pd single-atom catalysts on nitrogen-doped graphene for the highly selective photothermal hydrogenation of acetylene to ethylene. Adv. Mater. *31*, e1900509.

73. Wei, S., Li, A., Liu, J.C., Li, Z., Chen, W., Gong, Y., Zhang, Q., Cheong, W.C., Wang, Y., Zheng, L., et al. (2018). Direct observation of noble metal nanoparticles transforming to thermally stable single atoms. Nat. Nanotechnol. *13*, 856–861.

74. Pei, G.X., Liu, X.Y., Yang, X.F., Zhang, L.L., Wang, A.Q., Li, L., Wang, H., Wang, X.D., and Zhang, T. (2017). Performance of Cu-alloyed Pd single-atom catalyst for semihydrogenation of acetylene under simulated front-end conditions. ACS Catal. *7*, 1491–1500.

75. Pei, G.X., Liu, X.Y., Wang, A., Lee, A.F., Isaacs, M.A., Li, L., Pan, X., Yang, X., Wang, X., Tai, Z., et al. (2015). Ag alloyed Pd single-atom catalysts for efficient selective hydrogenation of acetylene to ethylene in excess ethylene. ACS Catal. *5*, 3717–3725.

76. Pei, G.X., Liu, X.Y., Wang, A., Li, L., Huang, Y., Zhang, T., Lee, J.W., Jang, B.W.L., and Mou, C.-Y. (2014). Promotional effect of Pd single atoms on Au nanoparticles supported on silica for the selective hydrogenation of acetylene in excess ethylene. New J. Chem. *38*, 2043–2051.

77. Jiao, L., and Regalbuto, J.R. (2008). The synthesis of highly dispersed noble and base metals on silica via strong electrostatic adsorption: I. Amorphous silica. J. Catal. *260*, 329–341.